Dalton Transactions

SPAAC iClick: Progress Towards a Bioorthogonal Reaction Incorporating Metal Ions

Journal:	*Dalton Transactions*
Manuscript ID	DT-ART-08-2021-002626
Article Type:	Paper
Date Submitted by the Author:	06-Aug-2021
Complete List of Authors:	Shen, Yu-Hsuan; University of Florida Esper, Alec; University of Florida Ghiviriga, Ion; University of Florida Abboud, Khalil; University of Florida, Department of Chemistry Schanze, Kirk; University of Texas at San Antonio College of Sciences, Chemistry Department Ehm, Christian; Frederico II University of Naples, Department of Chemical Sciences Veige, Adam; University of Florida, Chemistry

ARTICLE

SPAAC iClick: Progress Towards a Bioorthogonal Reaction Incorporating Metal Ions

Received 00th January 20xx,
Accepted 00th January 20xx

DOI: 10.1039/x0xx00000x

Yu-Hsuan Shen,[a] Alec M. Esper,[a] Ion Ghiviriga,[a] Khalil A. Abboud,[a] Kirk S. Schanze,[c] Christian Ehm,*[b] Adam S. Veige.*[a]

Combining strain-promoted azide-alkyne cycloaddition (SPAAC) and inorganic click (iClick) reactivity provides access to metal 1,2,3-triazolates. Experimental and computational insights demonstrate that iClick reactivity of the tested metal azides (LM-N_3, M = Au, W, Re, Ru and Pt) depends on the accessibility of the azide functionality rather than electronic effects imparted by the metal. SPAAC iClick reactivity with cyclooctyne is observed when the azide functionality is sterically unencumbered, e.g. [Au(N_3)(PPh_3)] (**Au-N_3**), [W(η^3-allyl)(N_3)(bpy)($CO)_2$] (**W-N_3**), and [Re(N_3)(bpy)$(CO)_3$] [bpy = 2,2'-bipyridine] (**Re-N_3**). Increased steric bulk and/or preequilibria with high activation barriers prevent SPAAC iClick reactivity for the complexes [Ru(N_3)(Tp)$(PPh_3)_2$] [Tp = tris(pyrazolyl)borate] (**Ru-N_3**), [Pt(N_3)$(CH_3)(P^iPr_3)_2$] [^{i}Pr = isopropyl] (**Pt(II)-N_3**), and [Pt(N_3)$(CH_3)_3]_4$ (**$(PtN_3)_4$**). Based on these computational insights, the SPAAC iClick reactivity of [Pt(N_3)$(CH_3)_3(P(CH_3)_3)_2$] (**Pt(IV)-N_3**) was successfully predicted.

Introduction

Manipulating chemistry within living cells requires absolute control of reactivity considering the milieu of functionality, biochemical machinery, and molecular complexity. Bioorthogonal chemistry excludes deleterious side-reactions, thus giving confidence to the end-user by guaranteeing the desired chemical outcome. Copper-catalyzed azide–alkyne cycloadditions (CuAAC), a variant of Huisgen's 1,3-dipolar cycloadditon,[1,2] are bioorthogonal.[3,4] However, the cytotoxicity of copper limits some applications.[5–7] Developing other bioorthogonal reactions continues to be an open area of research,[7–11] but the azide-alkyne cycloaddition and its superior features are simply too good[12] to abandon.

Spring loading reactions by destabilizing the ground state energy of the participating reagents is an effective approach to developing bioorthogonal reactions. Strain-promoted azide-alkyne cycloaddition (SPAAC), exemplifying this strategy, loads potential into the strain energy of cyclic alkynes. Cyclooctyne, for example, stores 19.9 kcal/mol of strain according to strain-energy calculations at the B3LYP/6-311+G(3df,2p) level.[13] As a consequence, SPAAC is spontaneous and fast,[7,14–16] whereas classical Huisgen's azide-alkyne cycloaddition is spontaneous and slow. Although CuAAC is also spontaneous and fast, it requires a Cu(I) catalyst. Imaging (drug,[18,19] protein,[17–21] glycan[22–26]), labelling (oligonucleotide,[27–29] protein[30]), and drug delivery,[31–33] are some of the numerous applications of SPAAC and span *in vitro*, *in vivo*, and *ex vivo*[33] methods. Removing Cu(I) in azide-alkyne cycloadditions is important for applications where side-effects from Cu(I) poisoning or interference are known.[34,35] However, deliberately and controllably incorporating metal ions into living systems is an expanding area of research with broad potential for the obvious reason that the properties of metal ions are infinitely tuneable by choice of metal ion, oxidation state, and ancillary ligand, and are thus promising pharmacological materials to treat *e.g.* cancer, malaria and neurodegenerative diseases.[36–40]

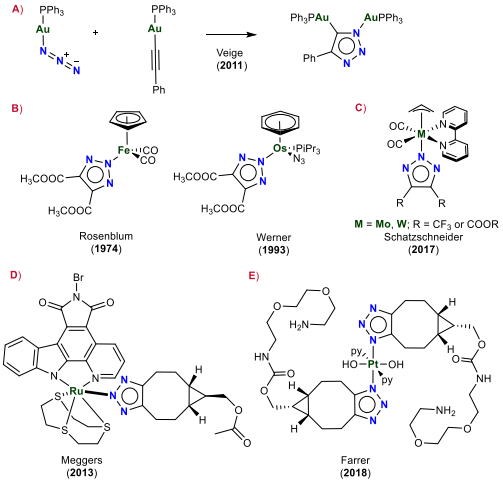

Scheme 1. (A) Original iClick reaction of linear gold(I) azido complex with a gold(I) acetylide, **(B)** early and **(C)** recent examples of octahedral 1,2,3-triazolate complexes from cycloaddition reactions of electron-poor alkynes, **(D)** and **(E)** first examples of a SPAAC iClick derived metal 1,2,3-triazolates using cyclooctyne bicyclo[6.1.0]non-4-yne (**BCN**) derivatives.

[a] *University of Florida, Department of Chemistry, Center for Catalysis, P.O. Box 117200, Gainesville, FL, 32611.*
[b] *Dipartimento di Scienze Chimiche, Università di Napoli Federico II, Via Cintia, 80126 Napoli, Italy.*
[c] *University of Texas at San Antonio, Department of Chemistry, One UTSA Circle, San Antonio, TX 78249.*

† Electronic supplementary information (ESI) available: Experimental details: Tables S1–S5, and Fig. S1–S27. Computational Details: Tables S6-24, and Fig. S28-S31. CCDC 2068053-2068056 and 2069850. For ESI and crystallographic data in CIF and other electronic format see DOI: 10.1039/x0xx00000x

Needed for the toolbox is a bioorthogonal reaction that controllably incorporates metal ions into living systems while maintaining the preconditions of easy synthesis and reliability for the end-user. Inorganic Click (iClick)[41] incorporates metal ions into the classic azide-alkyne cycloaddition and is an obvious choice for developing a metal centered bioorthogonal reaction.[41–44] Some of the first examples of cycloadditions within the coordination sphere of metals ions date to the mid-1970's.[45,46] However, the reaction of a metal-azide and a metal-acetylide to give a bimetallic complex was only recently reported (Scheme 1A).[41] Overwhelmingly since that report, alkyne (dipolarophile) activation using strongly electron withdrawing substituents, for example carboxylic esters or nitriles, has been the focus (Scheme 1B and 1C).[47–53]

Tuning of the alkyne with electron-withdrawing substituents accelerates the cycloaddition by facilitating formation of the metal ion π-complex and allows for mild reaction conditions, a prerequisite for bioorthogonality.[49,50,54–59] Rarely exploited, Meggers et al. reported one case of using SPAAC to promote the cycloaddition between cyclic alkynes and a Ru-azide (Scheme 1D). In the study, a cyclooctyne bicyclo[6.1.0]non-4-yne (**BCN**) derivative, featuring a fused cyclopropane ring, reacts rapidly due to significant ring strain yielding a Ru-1,2,3-triazolate complex (henceforth simplified to triazolate). In contrast, the less strained 3-methoxycyclooct-1-yne does not react.[60] Farrer and co-workers demonstrated another example of **BCN** cycloaddition with *trans*,*trans*,*trans*-$[Pt(N_3)_2(OH)_2(py)_2]$ to form mono- and bistriazolate complexes (Scheme 1E).[61] This raises two fundamental questions: (1) is the lack of reactivity with low-strain substrates general and SPAAC iClick limited to only extremely strained substrates, and (2) what features (electronic structure, sterics) of the metal-azide determine successful and rapid SPAAC iClick reactions. In this work, representative mid-to-late transition metal azide complexes that vary in steric congestion from groups 6 (W), 7 (Re), 8 (Ru), 10 (Pt) and 11 (Au) and non-functionalized cyclooctyne are the subject of computational and experimental SPAAC interrogation (Scheme 2).

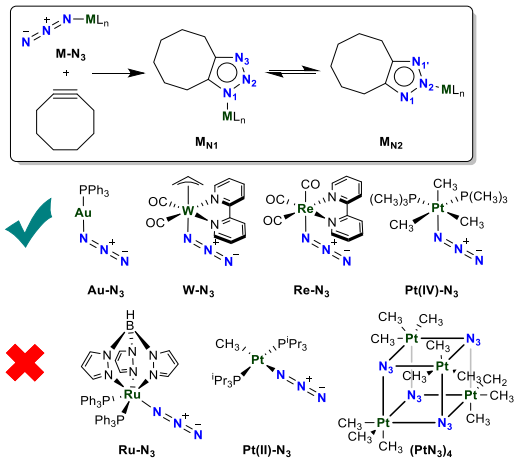

Scheme 2. Top: General M-azide/cyclooctyne probe reaction yielding ML_n-2-triazolate and/or ML_n-1-triazolate complexes. **Bottom**: M-azide complexes tested and the SPAAC iClick outcome.

Cyclooctyne is the target substrate rather than higher-strain derivatives, such as **BCN,** because the expectation is that success with cyclooctyne will translate broadly to more reactive substrates. The results provide necessary insights for both the development of iClick bioorthogonality and predictive modeling for SPAAC iClick reactivity. This work provides new insight into a generalized bioorthogonal reaction incorporating metal ions.

Results and Discussion

SPAAC iClick reactivity study. Synthesized according to literature procedures, seven metal-azides spanning groups 6-11 were chosen to probe SPAAC iClick. Scheme 2 describes the general reaction that combines L_nM-azides with cyclooctyne to yield L_nM-2-triazolates and/or L_nM-1-triazolates. Of the six complexes tested initially, $[Au(N_3)(PPh_3)]$ (**Au-N₃**), $[W(\eta^3\text{-allyl})(N_3)(bpy)(CO)_2]$ (**W-N₃**), $[Re(N_3)(bpy)(CO)_3]$ (**Re-N₃**), $[Pt(N_3)(CH_3)_3(P(CH_3)_3)_2]$ (**Pt(IV)-N₃**) result in successful cycloadditions, whereas $[Ru(N_3)(Tp)(PPh_3)_2]$ (**Ru-N₃**), and $[Pt(N_3)(CH_3)(P^iPr_3)_2]$ (**Pt(II)-N₃**) do not react with cyclooctyne. The SPAAC iClick reactivity of $[Pt(N_3)(CH_3)_3(P(CH_3)_3)_2]$ (**Pt(IV)-N₃**), tested as a proof-of-concept, is described later on.

[Au(N₃)(PPh₃)]. Complex **Au-N₃** reacts with cyclooctyne (1.2 equiv) in THF at ambient temperatures to produce $\mathbf{Au_{N1}}$, eventually isomerizing to $\mathbf{Au_{N2}}$ as a yellow solid in 94% isolated yield (Figure 1). The process of isomerization is slow enough to allow crystallization of the kinetic product. Diffusion of pentane into a THF solution of a mixture of $\mathbf{Au_{N1}}$ and $\mathbf{Au_{N2}}$ yields $\mathbf{Au_{N1}}$ single crystals suitable for X-ray diffraction. Figure 1 depicts the crystal structure of $\mathbf{Au_{N1}}$ featuring the triazolate ring binding to the gold metal through the N1 atom. Terminal alkyne cycloadditions with **Au-N₃** produces C-bound triazolates,[44,62] yet this is impossible in the bicyclic product derived from cyclooctyne. Therefore, the N-bound persists. Products $\mathbf{Au_{N1}}$ and $\mathbf{Au_{N2}}$ lend support to formation of initial N-bound products followed by isomerization in the original cycloadditions explored by Gray et al.[63]

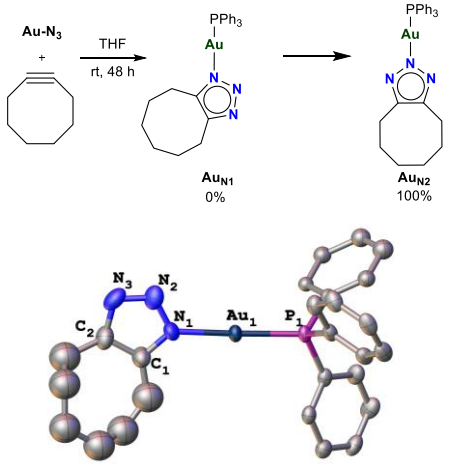

Figure 1. Synthesis and molecular structure of $\mathbf{Au_{N1}}$ with ellipsoids drawn at the 50% probability level and hydrogen atoms removed for clarity. Selected bond lengths (Å) and angles (°) for $\mathbf{Au_{N1}}$: Au1– N1 2.061(4), N1–N2 1.299(7), N2–N3 1.258(7), N1–C1 1.334(7), N3–C2 1.389(8), ∠N1–Au1–P1 177.01(13), ∠Au1–N1–N2 119.80(3), ∠Au1–N1–C1 131.00(4), ∠N1–N2–N3 113.60(5).

The ^{1}H NMR spectrum of a freshly synthesized mixture of **Au_{N1}/Au_{N2}** is complex and features multiple broad signals and evidence that additional unidentified intermediates are present. However, **Au_{N2}** becomes the dominant species and once isolated the ^{1}H NMR spectrum exhibits only three signals in the aliphatic region attributable to the hydrogen atoms on the cyclooctyl-triazolate ligand at 2.90, 1.75, and 1.47 ppm. Resonating as a singlet in the ^{31}P{^{1}H} NMR spectrum P-atom in the PPh_3 ligand appears at 33.3 ppm. Evidence for a successful SPAAC iClick reaction, the ^{13}C{^{1}H} NMR spectrum of **Au_{N2}** contains a diagnostic singlet resonance at 142.7 ppm attributable to the sp^2-carbons of the triazolate.

[W(η^3-allyl)(N_3)(bpy)($CO)_2$]. Treating **W-N_3** with 1.2 equiv of cyclooctyne in DMSO at room temperature for three days in the dark provides the triazolate SPAAC iClick product **W_{N2}** as a brown-red powder in 58% isolated yield. Rearrangement of the initial N1 isomer (**W_{N1}**) in solution must be fast since the N2 bound tungsten triazolate is the sole observable product by NMR spectroscopy (Figure 2). The ^{1}H NMR spectrum of **W_{N2}** exhibits three resonances at 2.32, 1.32, and 1.14 ppm for the methylene protons on the cyclooctyl moiety, indicating a pseudo-C_s-symmetry with the symmetry plane bisecting the bicyclic moiety and fast rotation around the W-N2 bond. Suggesting a symmetric environment around the ligand as well, signals at δ 8.70, 8.59, 8.19, and 7.54 ppm are attributable to the bipyridine (bpy) ligand. The ^{13}C{^{1}H} NMR spectrum of **W_{N2}** also supports this assignment; four signals appear at δ 143.0, 27.8, 25.5, and 21.3 ppm for the carbon atoms on the cyclooctyl-triazolate ligand.

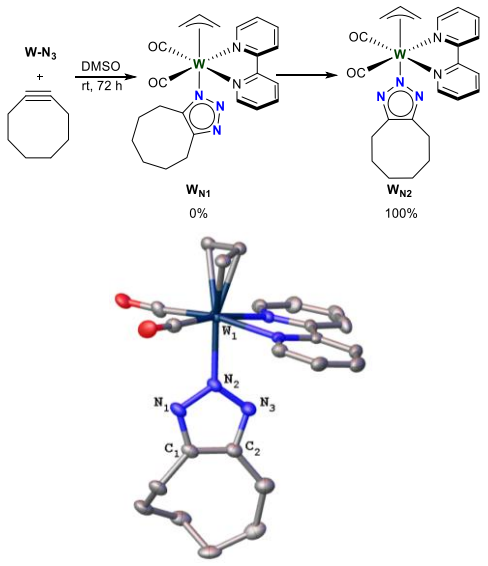

W_{N1} 0% W_{N2} 100%

Figure 2. Synthesis and molecular structure of **W_{N2}** with ellipsoids drawn at the 50% probability level and hydrogen atoms removed for clarity. Selected bond distances (Å): W1–N2 2.155(2), N1–N2 1.355(3), N2–N3 1.343(3), N1-C1 1.340(4), N3-C2 1.342(4). Selected bond angles (°): ∠W1–N2–N3 125.85(17), ∠W1–N2–N1 122.20(18), ∠N2–N3–C2 106.20(2), ∠N2–N1–C1 106.10(2).

Providing conclusive evidence of the triazolate connectivity (Figure 2), layering a concentrated acetone solution of **W_{N2}** with pentane precipitates hickory-colored crystals amenable to single crystal X-ray diffraction. C_1-symmeric in the solid state, the plane of the triazolate ring is perpendicular to the bpy plane. Exhibiting an octahedral geometry, the W-coordination sphere contains *cis*-carbonyls *trans* to the bpy ligand and *trans*-disposed allyl and triazolate ligands.

[Re(N_3)(bpy)($CO)_3$]). Prepared for the first time, mixing [ReCl(bpy)($CO)_3$][64] with sodium azide and silver triflate at room temperature in a mixture of THF: MeOH (1:1 v/v) for one day provides **Re-N_3** in 59% yield. Combining **Re-N_3** and cyclooctyne (1.2 equiv) in DMSO at room temperature for 8 d in the dark yields a mixture of N1 and N2 bound metal triazolate SPAAC iClick products, **Re_{N1}** and **Re_{N2}**, as a yellow powder in 87% yield (Figure 3). Multinuclear NMR spectra are consistent with an equilibrium mixture of isomers **Re_{N1}** and **Re_{N2}** in a 1:1.8 ratio (25 °C). Complex **Re_{N1}** forms initially as the kinetic product after 24 h followed by gradual isomerization. The reaction was monitored for another 3 d after workup and no change of the ratio was observed.

Complexes **Re_{N1}** and **Re_{N2}** are inseparable by fractional crystallization. The ^{1}H NMR spectrum displays two sets of signals, one contains seven larger signals attributable to the symmetric major isomer **Re_{N2}**, the other set with smaller signals belonging to the asymmetrical minor isomer **Re_{N1}**. Indicative of pseudo-C_s-symmetry with the symmetry plane bisecting the bicyclic moiety and fast rotation around the Re-N2 bond, the ^{1}H NMR spectrum of **Re_{N2}** (DMSO-d_6) displays four signals in the aromatic region corresponding to the bpy moiety at δ 9.06, 8.62, 8.27, and 7.71 ppm, and three signals in the aliphatic region corresponding to the cyclooctyl methylene protons at δ 2.33, 1.32 and 1.11 ppm. Depicted in Figure S12, **Re_{N1}** displays a more complex ^{1}H NMR spectrum. Consistent with the structural assignment and symmetry, the ^{15}N gHMBC NMR spectrum reveals a signal at 349.8 ppm attributable to the N1 and N1' on the triazolate ring on complex **Re_{N2}**, while complex **Re_{N1}** displays two signals at 351.9 (N3) and 267.1 ppm (N1).

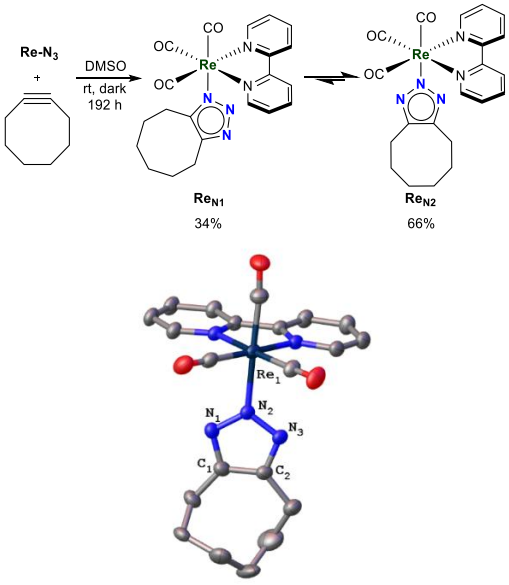

Re_{N1} 34% Re_{N2} 66%

Figure 3. Synthesis and molecular structure of **Re_{N2}** with ellipsoids drawn at the 50% probability level and hydrogen atoms removed for clarity. Selected bond distances (Å): Re1–N2 2.150(2), N1–N2 1.337(3), N2–N3 1.345(3), N3–C2 1.343(3), N1–C1 1.351(4). Selected bond angles (°): ∠Re1–N2–N3 122.88(16), ∠Re1–N2–N1 124.61(17), ∠N2–N1–C1 105.70(2), ∠ N2–N3–C2 105.60(2).

Vapor diffusion of pentane into a concentrated solution of the isomers in acetone precipitates a mixture of crystals. X-ray data collected on a crystal selected from the mixture reveals the molecular structure of **Re_{N2}** (Figure 3). The complex is octahedral with the bpy ligand and two of the *fac*-CO ligands opposite each other. In contrast to **W_{N2}**, the triazolate ring is perpendicular to the mirror plane of the complex. Unprecedented for metal triazolate complexes is the observation of an ambient temperature equilibrium mixture of N1/N2 triazolate isomers (**Re_{N1}**/**Re_{N2}**) i.e., slow equilibrium with only minimal preference for one of the isomers in solution. Schatzschneider reported a rare example for very slow, but irreversible rearrangement.[65] It was anticipated that **Re_{N1}** and **Re_{N2}** would exhibit photoluminescence from a metal-to-ligand charge transfer excited state. However, photoluminescence measurements revealed at best only a very weak emission (quantum yield < 0.001).

[Ru(N$_3$)(Tp)(PPh$_3$)$_2$], [Pt(N$_3$)(CH$_3$)(P^{i}Pr$_3$)$_2$], and Pt(N$_3$)(CH$_3$)$_3$. Complexes **Ru-N_3**, **Pt(II)-N_3**, and **$(PtN_3)_4$** do not react with 1.2 equiv of cyclooctyne in C_6D_6, even after 2 weeks at ambient temperatures. Increasing the reaction temperature to 50 °C and addition of CuOAc both fail to yield the triazolates. Emphasizing the lack of reactivity, quantitative recovery of the starting metal azide is possible in all cases.

N1/N2 isomerism. Huisgen's 1,3-dipolar cycloaddition produces solely 1-triazolates. Migration of the N-R group to the N2 position does not occur,[66,67] though an example of migration upon addition of MeI was demonstrated.[68] 1-Triazolates are, in all cases, the kinetic products upon iClick; however, only the original dinuclear Au_2-triazolates (Scheme 1)[41] retain that regiochemical outcome. Under basic conditions rather than iClick, adding benzotriazole to PPh_3AuCl yields the N1-isomer,[69] all other examples isomerize to the 2-triazolate.[48,51,60] Similarly, 2H-1,2,3-triazoles are the major isomer in aqueous solution.[70] In this study, **Au-N_3**, **W-N_3**, and **Pt(IV)-N_3** ultimately yield the 2-triazolate product. Clearly, the factors tilting thermodynamic preference are not always obvious since **Au-N_3** initially produces **Au_{N1}** (X-ray structure), and for **Re-N_3**, both isomers, **Re_{N1}** and **Re_{N2}**, are nearly equal in energy (1:2 ratio) and are observable by ^{1}H NMR spectroscopy.

DFT calculations at the B3LYP-D0(PCM)/TZ //B3LYP/DZ level of theory (see SI for details and references)[71–92] interrogate the N1/N2 isomerism. Bond lengths and angles of computationally optimized metal azides and resulting triazolates are in good agreement with available X-ray crystal structures (see SI).[41,48,55,93] Consistent with the synthetic outcome and timescale for the reaction, the computed Gibbs free energy of **Au_{N2}** is 1.3 kcal/mol lower than the **Au_{N1}** isomer in THF and the barrier for isomerization $\Delta G^{\ddagger}_{298K,\ THF}$ = 17.7 kcal/mol. Again, consistent with observations, the calculations predict a rapid interconversion barrier for **W_{N1}** → **W_{N2}** ($\Delta G^{\ddagger}_{298K,\ DMSO}$ = 15.4 kcal/mol), and that **W_{N2}** is the thermodynamic product ($\Delta G_{298K,\ DMSO}$ = -2.9 kcal/mol) with an equilibrium constant K_{eq} of 133. Accordingly, **W_{N2}** is the only observable product. In contrast, the computed interconversion barrier for **Re_{N1}** → **Re_{N2}** is considerably higher ($\Delta G^{\ddagger}_{298K,\ DMSO}$ = 19.2 kcal/mol), in line with the observed longer timescale to reach equilibrium. In agreement with experimental results, the computed preference for **Re_{N2}** is 1.3 kcal/mol ($\Delta G_{298K,\ DMSO}$). Validating the computational approach, the preference determined by experiment is 0.4 kcal/mol.

Factors determining SPAAC iClick reactivity. The disparity in SPAAC iClick reactivity of metal azides in this study indicates success depends intimately on the metal complex. The goal is to develop fundamental principles for SPAAC iClick to rival the organic version. The first step is to develop a predictive computational protocol with the same level of theory that successfully predicts the N1/N2 isomerism. We modelled the SPAAC iClick potential energy surface by DFT to examine the roots of M-N_3 reactivity.

Barriers for organic SPAAC reactions with cyclooctynes range between ~8-25 kcal/mol, depending on the choice of substituents and stereochemistry at the propargyl position.[66,94–96] Figure 4A depicts the cycloaddition between methyl azide/2-butyne and methyl azide/cyclooctyne and relates the predistortion and orbital energy reorganization to the observed low barrier cyclic alkynes. It is obvious from the starting cycloalkyne that ring strain forces the alkyne to distort to 157.2°, whereas for the linear alkyne the angle starts, as expected, at 180°. Both approach the transition state with angles of approximately 155°. This distortion requires 10.5 kcal/mol for 2-butyne but a mere 2.8 kcal/mol for cyclooctyne. Hence, the preexisting distortion in cycloctyne and a corresponding ground state destablization greatly accelerate the rate, requiring only minutes at ambient temperatures. Without this predistortion, linear alkynes require either a change in mechanism by using a Cu-catalyst or high temperatures (>100 °C) coupled with long reaction times.[67] Additionally, predistortion primes the alkyne frontier molecular orbitals (FMO) for the 1,3-dipolar cycloaddition (Figure 4B). Distortion changes the LUMO orbital symmetry and increases the orbital lobe size of the frontier molecular orbitals (FMO) on the concave side (i.e., the accessible side) of the strained triple bond. Finally, as demonstrated by Houk and Bickelhaupt, this distortion also leads to enhanced orbital stabilization in the TS and increased orbital overlap with the reacting azide.[96]

The calculated barrier for triazolate formation is 23 ± 1 kcal/mol for metal azides **Au-N_3**, **Re-N_3**, and **W-N_3**, similar to barriers for organic azides that proceed at room temperature with cyclooctyne (*vide supra*). Instead, for **Ru-N_3** and **Pt(II)-N_3**, the barrier increases substantially (by 7-9 kcal/mol, see SI), corresponding to a rate decrease of 6-8 orders of magnitude. FMO and steric hindrance analysis provides insight into the origin of the kinetic barrier increase.

Azide Role: FMO analysis. HOMO and LUMO energies, orbital symmetries, and HOMO-LUMO gaps – both for normal and inverse electron demand SPAAC iClick reactions of alkynes and metal azides – indicate no general trend to explain the lack of reactivity of **Ru-N_3** and **Pt(II)-N_3** (see SI). HOMO-LUMO gaps between all metal azides and cyclooctyne for both normal (5-7 eV) and inverse electronic (4-6 eV) are actually lower than those reported for organic SPAAC reactions (7-10 eV).[96]

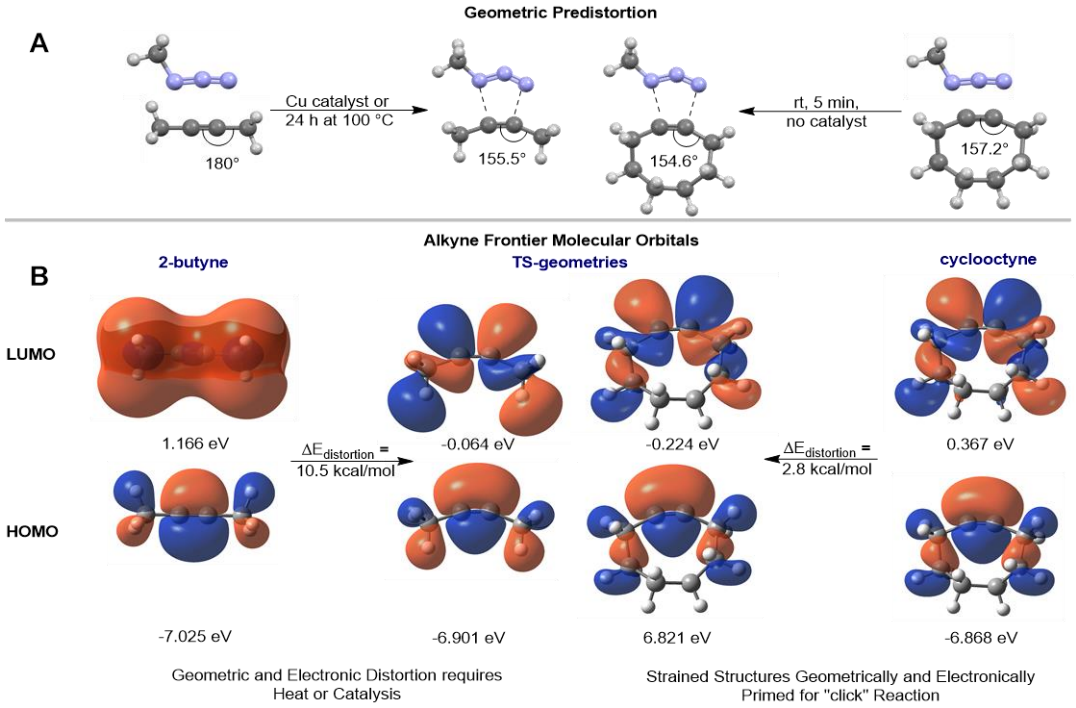

Figure 4. (A) SPAAC reactions are accelerated due to electronic and geometric predistortion. C-C-C bond angles in cyclooctyne are already at TS state geometry while 2-butyne requires a ~25° change. **(B)** FMO orbitals of cyclooctyne are already primed and the correct LUMO symmetry for 2-butyne is only attained by significant distortion. FMO pictures generated from B3LYP-D0(PCM)/TZ single point energy calculations using GaussView 6, isovalue 0.02).[97]

Changing the phosphine in **Ru-N_3** from triphenyl to more electron donating trimethyl phosphine does not result in a marked change in FMO energies, neither does a similar change for **Pt(II)-N_3**. Clearly, other factors are influencing the reactivity disparity.

Azide Role: Analysis of steric hindrance. Cavallo's SambVca 2.0 program[98] provides topographic maps of the steric hindrance around the azide N1 atom for all the metal azide complexes interrogated. SambVca 2.0 analyzes the distribution of steric bulk around a reactive site using a scanning sphere of adjustable radius and converts this into a topographical map (blue to red represents increasing steric bulk) and a single 3D-steric descriptor that measures the space occupied by the ligand framework in the designated sphere (buried volume, %V_{Bur}).[99] A common application is to examine the catalytic pockets from the perspective of the metal. SambVca analyses the distribution of steric bulk in various areas of the ligand framework (see references for examples).[100–102] Here, the reactivity centers on the azide functionality and the metal is only a spectator.

Using a 5.0 Å scanning sphere on the N1-atom probes how the distribution of ligand steric bulk surrounding the metal azide influences the 1,3-dipolar cycloaddition (Figure 5B). Steric bulk in this region can interfere with the approaching cyclooctyne. Figure 5A depicts the calculated steric maps with overlayed optimized structures and %V_{bur}. The topographic steric maps of azides **Re-N_3**, **W-N_3**, and **Au-N_3** imply little to no steric interference with an approaching cyclooctyne (Figure 5A, no orange or red regions, %V_{bur} < 50%), consistent with the lower barriers. The lower steric congestion is obvious for **Au-N_3**, where the bulky triphenyl phosphine group is opposite to the reacting azide. The bipyridine ligands in **Re-N_3** and **W-N_3** lie flat in the meridional plane, inducing minimal steric pressure towards the azide region of space. All three cases yield ample space around the azide functionality for the approaching cyclooctyne. Conversely, the bulky phosphine substituents in **Ru-N_3** (PPh_3) and **Pt(II)-N_3** (P^iPr_3) lead to a concentration of significant steric bulk at the azide and interfere with the approaching cyclooctyne. (Figure 5A, indicated by orange and red regions and %V_{bur} > 50%). Presumably, the positive Van der Waals dispersion forces are not enough to compensate for the negative interactions.[103]

Variation of the steric hindrance around the metal azides **Au-N_3**, **Ru-N_3**, and **Pt(II)-N_3**, by replacing the large phosphine ligands with less bulky $P(CH_3)_3$ provides further insight into the influence of steric bulk on the activation barriers. For **Au-N_3**, where the phosphine ligand is far away from the azide, the change does not affect the activation barrier (within the accuracy of the applied method, Figure 6, right). Switching to smaller phosphines ligands induces dramatic changes for **Ru-N_3** and **Pt(II)-N_3** (Figure 6, left for **Pt(II)-N_3** and SI for **Ru-N_3**). First, the smaller phosphine lowers the activation barriers by ~-8 kcal/mol for **Pt(II)-N_3** and **Ru-N_3**. Secondly, the exergonicity of the dipolar addition increases to a similar degree. An obvious reduction below the azide occurs and is plainly visible in topographic steric maps of the reduced models of **Pt(II)-N_3** and **Ru-N_3** (Figure 5A). These findings imply that steric hindrance is the sole dividing line for complexes that undergo successful SPAAC iClick with cyclooctynes.

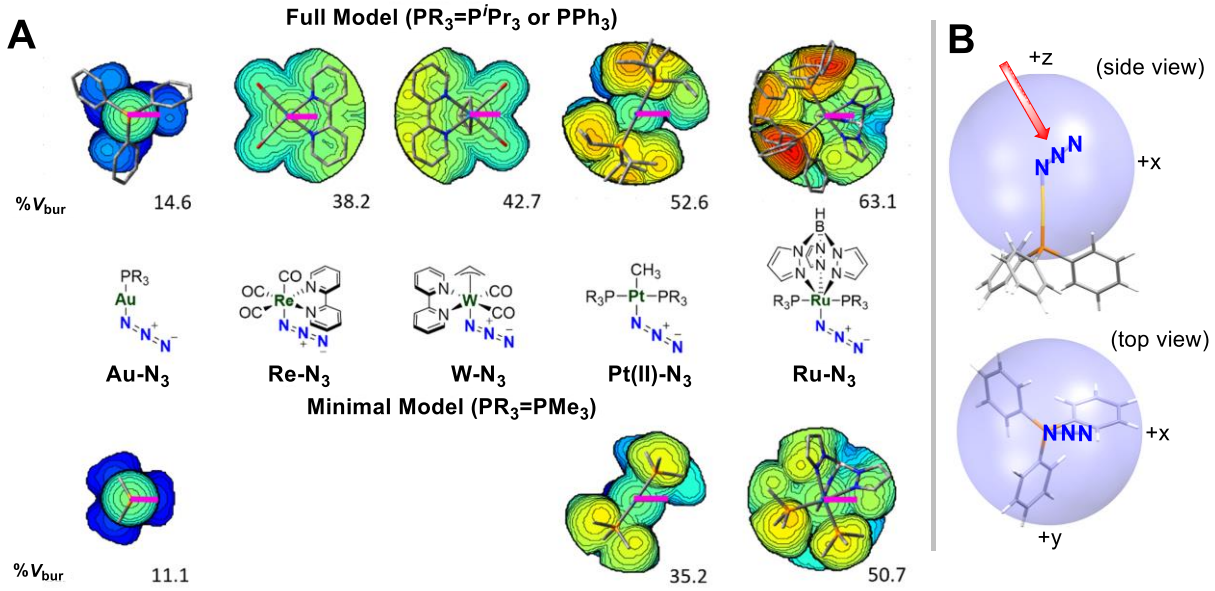

Figure 5. (A) Topographic maps of the steric hindrance around the azide N1 where cycloaddition occurs (azide centered to right and colored pink for emphasis; blue to red represents increasing steric bulk). Metal azides ordered by increasing %V_{bur}. Top row realistic models, bottom row, minimal models for complex **Au-N$_3$**, **Pt(II)-N$_3$**, and **Ru-N$_3$** (phosphine ligands replaced with P(CH$_3$)$_3$). **(B)** orientation of the coordinate system (z-axis: M-N1 bond, xz plane define by M-N1-N2) and location of the scanning sphere (5Å) on the example of Au-N$_3$; red arrow indicates approach vector of the cyclooctyne.

Pre-equilibrium Effect. The precursor of **Pt(II)-N$_3$** is **(PtN$_3$)$_4$**. Platinum IV prefers an octahedral coordination geometry, and as such, the complex exists in a tetrameric, cubane-like structure with alternating Pt and μ^2-end-on bridging azides on the cluster edges. Pt bridging halides and pseudohalides have been shown to be reactive,[104–106] and rhenium and tantalum end-on azides also demonstrate iClick reactivity.[107,108] Subjecting this tetramer to our steric analysis, **(PtN$_3$)$_4$** exhibits the highest %V_{bur} at 68.3% (see SI for steric map). The Pt(CH$_3$)$_3$ units shield the bridging azides, and thus, the calculated barrier for SPAAC iClick is prohibitively high (41.9 kcal/mol), in line with the experimentally observed lack of reactivity. Reaction via the monomeric form after dissociation requires only an activation energy of 21.4 kcal/mol. Although the calculated barrier for the monomeric form is similar to that of the reactive azides in this study, the energy necessary to generate the severely distorted monomer is prohibitively high (35.8 kcal/mol). This pre-equilibrium raises the barrier for the SPAAC iClick reaction to levels unattainable under the applied experimental conditions.

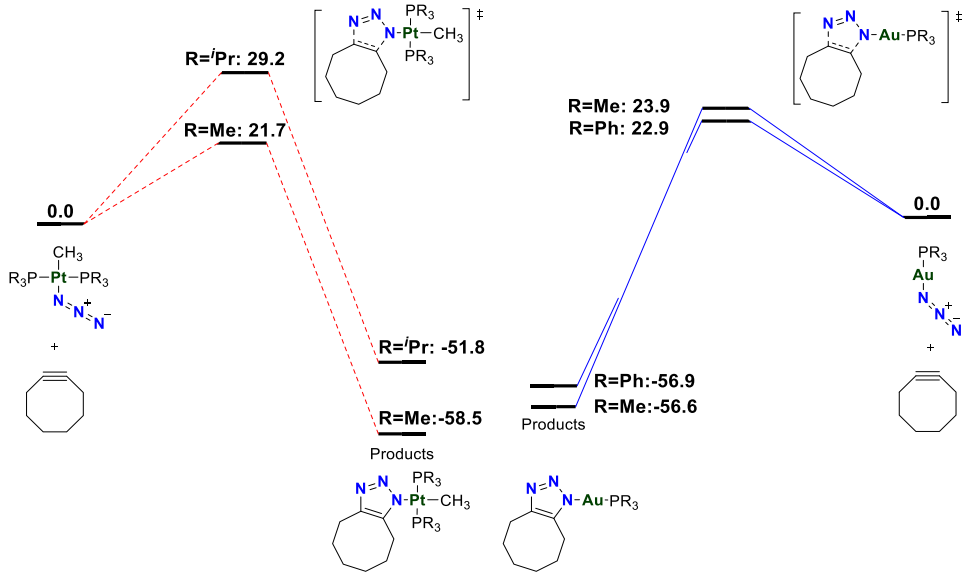

Figure 6. Computed potential energy surface (units in kcal/mol at 298K and 1 atm; calculated at B3LYP-D0(PCM)/TZ//B3LYP/DZ level of theory) of SPAAC reactions of **Pt(II)-N$_3$**(red, dashed) and **Au-N$_3$** (blue, solid). Replacing PPh$_3$ with the significantly smaller P(CH$_3$)$_3$ does not affect the barrier height for Au but replacing P^{i}Pr$_3$ has significant impact on the barrier for the Pt system, suggesting that sterics play an integral part in the SPAAC iClick reactivity of metal azide

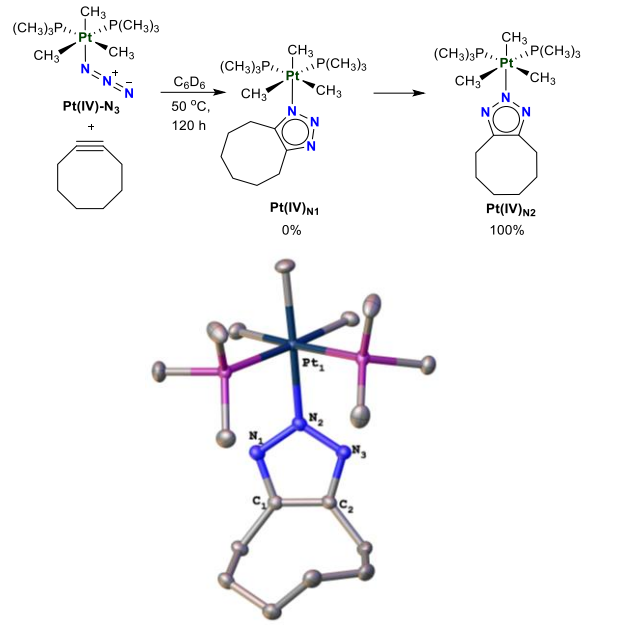

Figure 7. Synthesis and molecular structure of **Pt(IV)$_{N2}$** with ellipsoids drawn at the 50% probability level and hydrogen atoms removed for clarity. Selected bond distances (Å): Pt1–N2 2.128(2), N1–N2 1.345(3), N2–N3 1.337(3), N3–C2 1.350(3), N1–C1 1.352(3). Selected bond angles (°): ∠Pt1–N2–N3 123.92(16), ∠Pt1–N2–N1 122.09(16), ∠N2–N1–C1 105.20(2), ∠ N2–N3–C2 105.50(2).

In silico predictive power. One objective of this work is to advance SPAAC iClick by establishing parameters for predicting successful cycloaddition outcomes. **Pt(II)-N$_3$**, for steric reasons, and **(PtN$_3$)$_4$** (Scheme 2) due to sterics and a pre-equilibrium effect, are inert towards SPAAC iClick with cyclooctyne. Our model suggests a smaller version of **Pt(II)-N$_3$** and a mononuclear version of the tetramer **(PtN$_3$)$_4$** will react with cyclooctyne.

[Pt(N$_3$)(CH$_3$)$_3$(P(CH$_3$)$_3$)$_2$] (**Pt(IV)-N$_3$**) depicted in Figure 7 is mononuclear and contains the smaller P(CH$_3$)$_3$ phosphine ligand. Indeed, analysis of the steric environment for **Pt(IV)-N$_3$** (see SI for steric map) gives a %V_{bur} of 43.9 % (comparable to successful SPAAC iClick participants **Re-N$_3$** and **W-N$_3$**; see Figure 5). Moreover, DFT calculations predict a reasonable barrier for the cycloaddition for **Pt(IV)-N$_3$** of 23.2 kcal/mol. With an appropriate model selected, the synthesis of **Pt(IV)-N$_3$** and its reactivity with cyclooctynes was executed. Combining the tetramer **(PtN$_3$)$_4$**[109] with P(CH$_3$)$_3$ in toluene at 80 °C for 2 h yields **Pt(IV)-N$_3$** as a white solid in 60% yield. Layering a concentrated toluene solution of **Pt(IV)-N$_3$** with pentane induces precipitation of colorless crystals suitable for X-ray diffraction experiments. Figure S22 depicts the molecular structure and confirms the identity of **Pt(IV)-N$_3$**. Solution phase NMR data are also consistent with a mononuclear 6-coordinate complex containing *cis*-phosphines and *fac*-methyl ligands (see SI for spectra).

Treating **Pt(IV)-N$_3$** with 1.2 equiv of cyclooctyne in C$_6$D$_6$ at 50 °C for five days produces the triazolate iClick product **Pt(IV)$_{N2}$** in 13 % isolable yield, supporting the predictive modeling abilities of % V_{bur} and computed transition state barrier for SPAAC iClick reactivity. The N2 bound triazolate platinum complex **Pt(IV)$_{N2}$** is the sole product observed by NMR spectroscopy implying the N1/N2 rearrangement is fast consistent with the calculated energy difference between the two isomers ($\Delta G_{298K,\ benzene}$ = -2.4 kcal/mol).

The ^{1}H NMR spectrum of **Pt(IV)$_{N2}$** displays similar signals as the platinum azide precursor with an additional three resonances at 3.01, 1.75, 1.48 ppm for the methylene protons on the cyclooctyl-triazolate. The ^{31}P{^{1}H} NMR spectrum exhibits a singlet at -42.0 ppm, consistent with this assignment. The ^{13}C{^{1}H} NMR spectrum also demonstrates similar chemical shifts for the methyl and trimethyl phosphine groups on the platinum metal. Three additional singlets at 29.9, 26.0, and 24.4 ppm correspond to the methylene carbons on the cyclooctyl-triazolate. Moreover, the ^{13}C{^{1}H} NMR spectrum again displays a singlet resonance at 142.7 ppm attributable to the carbons of the triazolate ring, indicating a successful SPAAC iClick reaction.

Dissolving **Pt(IV)$_{N2}$** in pentane and cooling the solution to -25 °C pentane precipitates colorless crystals suitable for single crystal X-ray diffraction. The complex exhibited an octahedral geometry, with the two *cis*-CH$_3$ ligands and *cis*-PCH$_3$ ligands opposite each other, confirming the successful prediction for the SPAAC iClick reaction.

Conclusion

Reactions between metal azide complexes (**M-N$_3$**, M= Au, W, Re, Ru, Pt) from across the periodic table and cyclooctyne are model probes for SPAAC iClick. Only minimally sterically encumbered complexes (**Au-N$_3$**, **W-N$_3$**, **Re-N$_3$**, **Pt(IV)-N$_3$**) yield metal triazolates. **Ru-N$_3$** and **Pt(II)-N$_3$** with bulky phosphine ligands, do not react. Due to endergonicity of dissociation into mononuclear species, the tetramer **(PtN$_3$)$_4$** containing bridging azides is also unreactive.

The rhenium triazolate exists as a mixture of isomers **Re$_{N1}$**, and **Re$_{N2}$**, with the N2-triazolate slightly preferred. Previous examples of metal triazolates that form via iClick present as either the N1 or the N2 isomer, but not both. Unprecedented is the capturing of two isomers in equilibrium. The mixture of isomers offers an opportunity to calibrate DFT computations by comparing the measured equilibrium constant to calculation. Supporting an appropriate DFT methodology, the values are within 1 kcal/mol. There is also correlation between %V_{bur} and isomerization. For Au (smallest) the isomerization from N1 to N2 is slow, for Re (intermediate size) the isomers are in equilibrium, for W and Pt (largest) only the N2 isomer is isolable.

One important conclusion is the computational interrogation of the various complexes indicates a correlation between SPAAC iClick reactivity and accessibility of the azide substituent, electronic effects do not play a dominant role. The *a priori* selection and successful reaction between **Pt(IV)-N$_3$** and cyclooctyne provides proof-of-concept for the prediction and identification of suitable metal-azides for SPAAC iClick using DFT and/or 3D-geometric analysis of the N1 region with SambVca. Established already are thousands of syntheses for nearly every metal ion across the periodic table. Among the thousands of metal-azides are surely compounds that will fit the requirements to achieve bioorthogonality. Absolute control of reactivity in living cells requires the metal-azide to ignore the biochemical machinery and molecular complexity of living cells.

Incorporating metal ions will dramatically expand the synthetic and application scope of SPAAC. However, a systematic one-by-one experimental interrogation of each metal-azide is too daunting and arduous. This study establishes an approach for the rapid computational pre-screening of metal azides for reactivity with cyclooctynes. The simplicity of the single computational descriptor, i.e. a $\%V_{bur}$ less than 50% will greatly accelerate and narrow the search for metal-azides that participate in SPAAC iClick (Figure 8).

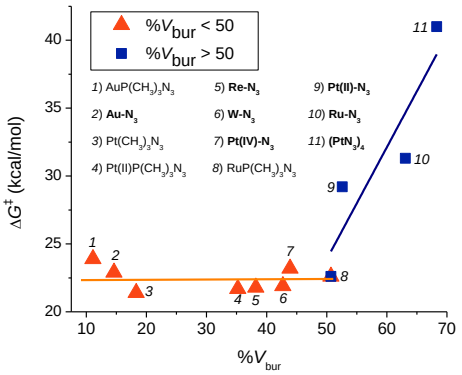

Figure 8. Plot of Calculated $\Delta G^{\ddagger}$ (kcal/mol) of SPAAC iClick vs. $\%V_{bur}$ for all structures investigated in this paper (bolded structures represent experimentally investigated azides). The orange line describes the average $\Delta G^{\ddagger}$ for azides with a $\%V_{bur}$<50 (23±1 kcal/mol) and navy line represents the linear relationship between $\Delta G^{\ddagger}$ of SPAAC iClick and $\%V_{bur}$ at $\%V_{bur}$>50. Passing 50 $\%V_{bur}$ results in a sharp barrier increase that prevents SPAAC iClick reactivity.

Conflicts of interest

There are no conflicts to declare.

Acknowledgements

Research supported by the U.S. Department of Energy, Office of Basic Energy Sciences, Division of Materials Sciences and Engineering under Award DE-SC0020008. The UF Mass Spectrometry Research and Education Center (NIH S10 OD021758-01A1) are thanked for acquisition of mass spectrometry data. K.A.A. acknowledges the NSF (CHE0821346) for the purchase of X-ray equipment. Analytical data were obtained from the CENTC Elemental Analysis Facility at the University of Rochester, funded by NSF CHE-0650456.

References

1 R. Huisgen, *Proc. Chem. Soc.*, 1961, 357–396.

2 R. Huisgen, *Angew. Chem. Int. Ed. Engl.*, 1968, **7**, 321–328.

3 C. C. Beto, Y. Yang, C. J. Zeman, I. Ghiviriga, K. S. Schanze and A. S. Veige, *Organometallics*, 2018, **37**, 4545–4550.

4 J. E. Hein and V. V. Fokin, *Chem. Soc. Rev.*, 2010, **39**, 1302–1315.

5 A. J. Link and D. A. Tirrell, *J. Am. Chem. Soc.*, 2003, **125**, 11164–11165.

6 E. Lallana, E. Fernandez-Megia and R. Riguera, *J. Am. Chem. Soc.*, 2009, **131**, 5748–5750.

7 E. M. Sletten and C. R. Bertozzi, *Angew. Chem. Int. Ed.*, 2009, **48**, 6974–6998.

8 R. D. Row and J. A. Prescher, *Acc. Chem. Res.*, 2018, **51**, 1073–1081.

9 D. M. Patterson, L. A. Nazarova and J. A. Prescher, *ACS Chem. Biol.*, 2014, **9**, 592–605.

10 T. Carell and M. Vrabel, *Top. Curr. Chem.*, 2016, 374, 1–21.

11 N. K. Devaraj, *ACS Cent. Sci.*, 2018, **4**, 952–959.

12 H. C. Kolb, M. G. Finn and K. B. Sharpless, *Angew. Chem. Int. Ed.*, 2001, **40**, 2004–2021.

13 R. D. Bach, *J. Am. Chem. Soc.*, 2009, **131**, 5233–5243.

14 N. J. Agard, J. A. Prescher and C. R. Bertozzi, *J. Am. Chem. Soc.*, 2004, **126**, 15046–15047.

15 J. Dommerholt, F. P. J. T. Rutjes and F. L. van Delft, *Top. Curr. Chem.*, 2016, **374**, 1–20.

16 J. C. Jewett and C. R. Bertozzi, *Chem. Soc. Rev.*, 2010, **39**, 1272–1279.

17 N. K. Devaraj, S. Hilderbrand, R. Upadhyay, R. Mazitschek and R. Weissleder, *Angew. Chem. Int. Ed.*, 2010, **49**, 2869–2872.

18 G. Budin, K. S. Yang, T. Reiner and R. Weissleder, *Angew. Chem. Int. Ed.*, 2011, **50**, 9378–9381.

19 K. S. Yang, G. Budin, T. Reiner, C. Vinegoni and R. Weissleder, *Angew. Chem. Int. Ed.*, 2012, **51**, 6598–6603.

20 E. Kim, K. S. Yang and R. Weissleder, *PLoS One*, 2013, **8**, 1–14.

21 A. Rutkowska, D. W. Thomson, J. Vappiani, T. Werner, K. M. Mueller, L. Dittus, J. Krause, M. Muelbaier, G. Bergamini and M. Bantscheff, *ACS Chem. Biol.*, 2016, **11**, 2541–2550.

22 P. V. Chang, J. A. Preschera, E. M. Sletten, J. M. Baskin, I. A. Miller, N. J. Agard, A. Lo and C. R. Bertozzi, *Proc. Natl. Acad. Sci. U. S. A.*, 2010, **107**, 1821–1826.

23 R. Xie, L. Dong, Y. Du, Y. Zhu, R. Hua, C. Zhang and X. Chen, *Proc. Natl. Acad. Sci. U. S. A.*, 2016, **113**, 5173–5178.

24 R. Rossin, P. R. Verkerk, S. M. Van Den Bosch, R. C. M. Vulders, I. Verel, J. Lub and M. S. Robillard, *Angew. Chem. Int. Ed.*, 2010, **49**, 3375–3378.

25 A. A. Neves, Y. A. Wainman, A. Wright, M. I. Kettunen, T. B. Rodrigues, S. McGuire, D. E. Hu, F. Bulat, S. Geninatti Crich, H. Stöckmann, F. J. Leeper and K. M. Brindle, *Angew. Chem. Int. Ed.*, 2016, **55**, 1286–1290.

26 S. Jawhara and S. Mordon, *Antimicrob. Agents Chemother.*, 2004, **48**, 3436–3441.

27 A. M. Pyka, C. Domnick, F. Braun and S. Kath-Schorr, *Bioconjugate Chem.*, 2014, **25**, 1438–1443.

28 F. Eggert and S. Kath-Schorr, *Chem. Commun.*, 2016, **52**, 7284–7287.

29 U. Reisacher, D. Ploschik, F. Rönicke, G. B. Cserép, P. Kele and H. A. Wagenknecht, *Chem. Sci.*, 2019, **10**, 4032–4037.

30 I. Nikić, G. Estrada Girona, J. H. Kang, G. Paci, S. Mikhaleva, C. Koehler, N. V. Shymanska, C. Ventura Santos, D. Spitz and E. A. Lemke, *Angew. Chem. Int. Ed.*, 2016, **55**, 16172–16176.

31 S. Lee, H. Koo, J. H. Na, S. J. Han, H. S. Min, S. J. Lee, S. H. Kim, S. H. Yun, S. Y. Jeong, I. C. Kwon, K. Choi and K. Kim, *ACS Nano*, 2014, **8**, 2048–2063.

32 H. Wang, R. Wang, K. Cai, H. He, Y. Liu, J. Yen, Z. Wang, M. Xu, Y. Sun, X. Zhou, Q. Yin, L. Tang, I. T. Dobrucki, L. W. Dobrucki, E. J. Chaney, S. A. Boppart, T. M. Fan, S. Lezmi, X. Chen, L. Yin and J. Cheng, *Nat. Chem. Biol.*, 2017, **13**, 415–424.

33 E. Kim and H. Koo, *Chem. Sci.*, 2019, **10**, 7835–7851.

34 D. Denoyer, S. Masaldan, S. La Fontaine and M. A. Cater, *Metallomics*, 2015, **7**, 1459–1476.

35 R. A. Festa and D. J. Thiele, *Curr. Biol.*, 2011, **21**, R877–R883.

36 C. Imberti and P. J. Sadler, *Adv. Inorg. Chem.*, 2020, **75**, 3–56.

37 S. Monro, K. L. Colón, H. Yin, J. Roque, P. Konda, S. Gujar, R. P. Thummel, L. Lilge, C. G. Cameron and S. A. McFarland, *Chem. Rev.*, 2019, **119**, 797–828.

38 L. Zeng, P. Gupta, Y. Chen, E. Wang, L. Ji, H. Chao and Z. S. Chen, *Chem. Soc. Rev.*, 2017, **46**, 5771–5804.

39 R. G. Kenny and C. J. Marmion, *Chem. Rev.*, 2019, **119**, 1058–1137.

40 N. P. E. Barry and P. J. Sadler, *Chem. Commun.*, 2013, **49**, 5106–5131.

41 T. J. Del Castillo, S. Sarkar, K. A. Abboud and A. S. Veige, *Dalton Trans.*, 2011, **40**, 8140–8144.

42 A. R. Powers, X. Yang, T. J. Del Castillo, I. Ghiviriga, K. A. Abboud and A. S. Veige, *Dalton Trans.*, 2013, **42**, 14963–14966.

43 L. Henry, C. Schneider, B. Mützel, P. V. Simpson, C. Nagel, K. Fucke and U. Schatzschneider, *Chem. Commun.*, 2014, **50**, 15692–15695.

44 C. J. Zeman, Y. H. Shen, J. K. Heller, K. A. Abboud, K. S. Schanze and A. S. Veige, *J. Am. Chem. Soc.*, 2020, **142**, 8331–8341.

45 W. P. Fehlhammer and W. Beck, *Z. Anorg. Allg. Chem.*, 2015, **641**, 1599–1678.

46 H. W. Frühauf, *Chem. Rev.*, 1997, **97**, 523–596.

47 P. V. Simpson, B. W. Skelton, P. Raiteri and M. Massi, *New J. Chem.*, 2016, **40**, 5797–5807.

48 P. Schmid, M. Maier, H. Pfeiffer, A. Belz, L. Henry, A. Friedrich, F. Schönfeld, K. Edkins and U. Schatzschneider, *Dalton Trans.*, 2017, **46**, 13386–13396.

49 F. C. Liu, Y. L. Lin, P. S. Yang, G. H. Lee and S. M. Peng, *Organometallics*, 2010, **29**, 4282–4290.

50 S. Miguel-Fernández, S. Martínez De Salinas, J. Díez, M. P. Gamasa and E. Lastra, *Inorg. Chem.*, 2013, **52**, 4293–4302.

51 K. Peng, R. Einsele, P. Irmler, R. F. Winter and U. Schatzschneider, *Organometallics*, 2020, **39**, 1423–1430.

52 A. Rosan and M. Rosenblum, *J. Organomet. Chem.*, 1974, **80**, 103–107.

53 T. Daniel, W. Knaup, M. Dziallas and H. Werner, *Chem. Ber.*, 1993, **126**, 1981–1993.

54 C. W. Chang and G. H. Lee, *Organometallics*, 2003, **22**, 3107–3116.

55 C. K. Chen, H. C. Tong, C. Y. C. Hsu, C. Y. Lee, Y. H. Fong, Y. S. Chuang, Y. H. Lo, Y. C. Lin and Y. Wang, *Organometallics*, 2009, **28**, 3358–3368.

56 P. Depe, O. C. O. Ome, G. Q. Li and M. Orchin, *J. Organomet. Chem.*, 1997, **535**, 43–47.

57 A. Dauth and J. A. Love, *Dalton Trans.*, 2012, **41**, 7782–7791.

58 P. Paul and K. Nag, *Inorg. Chem.*, 1987, **26**, 2969–2974.

59 A. R. Powers, I. Ghiviriga, K. A. Abboud and A. S. Veige, *Dalton Trans.*, 2015, **44**, 14747–14752.

60 T. Cruchter, K. Harms and E. Meggers, *Chem. Eur. J.*, 2013, **19**, 16682–16689.

61 N. J. Farrer, G. Sharma, R. Sayers, E. Shaili and P. J. Sadler, *Dalton Trans.*, 2018, **47**, 10553–10560.

62 X. Yang, S. Wang, I. Ghiviriga, K. A. Abboud and A. S. Veige, *Dalton Trans.*, 2015, **44**, 11437–11443.

63 D. V. Partyka, J. B. Updegraff, M. Zeller, A. D. Hunter and T. G. Gray, *Organometallics*, 2007, **26**, 183–186.

64 K. S. Schanze, D. Brent MacQueen, T. A. Perkins and L. A. Cabana, *Coord. Chem. Rev.*, 1993, **122**, 63–89.

65 K. Peng, V. Mawamba, E. Schulz, M. Löhr, C. Hagemann and U. Schatzschneider, *Inorg. Chem.*, 2019, **58**, 11508–11521.

66 D. H. Ess, G. O. Jones and K. N. Houk, *Org. Lett.*, 2008, **10**, 1633–1636.

67 Z. X. Wang and H. L. Qin, *Chem. Commun.*, 2003, **3**, 2450–2451.

68 L. N. Telegina, E. S. Kelbysheva, T. V. Strelkova, M. G. Ezernitskaya, Y. A. Borisov, A. F. Smol'yakov, A. S. Peregudov, A. N. Rodionov, N. S. Ikonnikov and N. M. Loim, *Eur. J. Org. Chem.*, 2016, **35**, 5897–5906.

69 D. Wang, Y. Zhang, R. Cai and X. Shi, *Beilstein J. Org. Chem.*, 2011, **7**, 1014–1020.

70 A. Albert and P. J. Taylor, *J. Chem. Soc., Perkin Trans. 2*, 1989, **11**, 1903–1905.

71 M. J. Frisch, G. W. Trucks, H. B. Schlegel, G. E. Scuseria, M. A. Robb, J. R. Cheeseman, G. Scalmani, V. Barone, B. Mennucci, G. A. Petersson, H. Nakatsuji, M. Caricato, X. Li, H. P. Hratchian, A. F. Izmaylov, J. Bloino, G. Zheng, J. L. Sonnenberg, M. Hada, M. Ehara, K. Toyota, R. Fukuda, J. Hasegawa, M. Ishida, T. Nakajima, Y. Honda, O. Kitao, H. Nakai, T. Vreven, J. A. Montgomery Jr., J. E. Peralta, F. Ogliaro, M. Bearpark, J. J. Heyd, E. Brothers, K. N. Kudin, V. N. Staroverov, R. Kobayashi, J. Normand, K. Raghavachari, A. Rendell, J. C. Burant, S. S. Iyengar, J. Tomasi, M. Cossi, N. Rega, J. M. Millam, M. Klene, J. E. Knox, J. B. Cross, V. Bakken, C. Adamo, J. Jaramillo, R. Gomperts, R. E. Stratmann, O. Yazyev, A. J. Austin, R. Cammi, C. Pomelli, J. W. Ochterski, R. L. Martin, K. Morokuma, V. G. Zakrzewski, G. A. Voth, P. Salvador, J. J. Dannenberg, S. Dapprich, A. D. Daniels, O. Farkas, J. B. Foresman, J. V Ortiz, J. Cioslowski and D. J. Fox, *Gaussian 09 Revis. C.01*, 2010, Gaussian Inc., Wallingford CT.

72 A. D. Becke, *J. Chem. Phys.*, 1993, **98**, 5648–5652.

73 H. P. Hratchian and H. B. Schlegel, *J. Chem. Theory Comput.*, 2005, **1**, 61–69.

74 J. Tomasi, *Theor. Chem. Acc.*, 2004, **112**, 184–203.

75 S. Grimme, *Wiley Interdiscip. Rev. Comput. Mol. Sci.*, 2011, **1**, 211–228.

76 S. Grimme, S. Ehrlich and L. Goerigk, *J. Comput. Chem.*, 2011, **32**, 1456–1465.

77 S. Tobisch and T. Ziegler, *J. Am. Chem. Soc.*, 2004, **126**, 9059–9071.

78 F. Zaccaria, C. Ehm, P. H. M. Budzelaar and V. Busico, *ACS Catal.*, 2017, **7**, 1512–1519.

79 F. Zaccaria, R. Cipullo, P. H. M. Budzelaar, V. Busico and C. Ehm, *J. Polym. Sci. Part A Polym. Chem.*, 2017, **55**, 2807–2814.

80 A. V. Marenich, C. J. Cramer and D. G. Truhlar, *J. Phys. Chem. B*, 2009, **113**, 6378–6396.

81 T. Yanai, D. P. Tew and N. C. Handy, *Chem. Phys. Lett.*, 2004, **393**, 51–57.

82 H. S. Yu, X. He, S. L. Li and D. G. Truhlar, *Chem. Sci.*, 2016, **7**, 5032–5051.

83 C. Lee, W. Yang and R. G. Parr, *Phys. Rev. B*, 1988, **37**, 785-789.

84 M. J. Frisch, G. W. Trucks, H. B. Schlegel, G. E. Scuseria, M. A. Robb, J. R. Cheeseman, G. Scalmani, V. Barone, G. A. Petersson, H. Nakatsuji, X. Li, M. Caricato, A. V. Marenich, J. Bloino, B. G. Janesko, R. Gomperts, B. Mennucci, H. P. Hratchian, J. V. Ortiz, A. F. Izmaylov, J. L. Sonnenberg, D. Williams-Young, F. Ding, F. Lipparini, F. Egidi, J. Goings, B. Peng, A. Petrone, T. Henderson, D. Ranasinghe, V. G. Zakrzewski, J. Gao, N. Rega, G. Zheng, W. Liang, M. Hada, M. Ehara, K. Toyota, R. Fukuda, J. Hasegawa, M. Ishida, T. Nakajima, Y. Honda, O. Kitao, H. Nakai, T. Vreven, K. Throssell, J. Montgomery, J. A., J. E. Peralta, F. Ogliaro, M. J. Bearpark, J. J. Heyd, E. N. Brothers, K. N. Kudin, V. N. Staroverov, T. A. Keith, R. Kobayashi, J. Normand, K. Raghavachari, A. P. Rendell, J. C. Burant, S. S. Iyengar, J. Tomasi, M. Cossi, J. M. Millam, M. Klene, C. Adamo, R. Cammi, J. W. Ochterski, R. L. Martin, K. Morokuma, O. Farkas, J. B. Foresman and D. J. Fox, *Gaussian 16 Revis. C.01, 2016, Gaussian, Inc., Wallingford, CT*.

85 J. Da Chai and M. Head-Gordon, *Phys. Chem. Chem. Phys.*, 2008, **10**, 6615–6620.

86 N. B. Balabanov and K. A. Peterson, *J. Chem. Phys.*, 2005, **123**, 64107.

87 N. B. Balabanov and K. A. Peterson, *J. Chem. Phys.*, 2006, **125**, 074110.

88 K. L. Schuchardt, B. T. Didier, T. Elsethagen, L. Sun, V. Gurumoorthi, J. Chase, J. Li and T. L. Windus, *J. Chem. Inf. Model.*, 2007, **47**, 1045–1052.

89 E. J. Baerends, D. E. Ellis and P. Ros, *Chem. Phys.*, 1973, **2**, 41–51.

90 J. L. Whitten, *J. Chem. Phys.*, 1973, **58**, 4496–4501.

91 M. Feyereisen, G. Fitzgerald and A. Komornicki, *Chem. Phys. Lett.*, 1993, **208**, 359–363.

92 O. Vahtras, J. Almlöf and M. W. Feyereisen, *Chem. Phys. Lett.*, 1993, **213**, 514–518.

93 S. Schlecht, N. Faza, W. Massa, S. Dapprich, G. Frenking and K. Dehnicke, *Z. Anorg. Allg. Chem.*, 1998, **624**, 1011–1014.

94 K. Chenoweth, D. Chenoweth and W. A. Goddard, *Org. Biomol. Chem.*, 2009, **7**, 5255–5258.

95 S. Ghandiyar, M. Hamzehloueian and R. Hosseinzadeh, *Struct. Chem.*, 2017, **28**, 1969–1979.

96 T. A. Hamlin, B. J. Levandowski, A. K. Narsaria, K. N. Houk and F. M. Bickelhaupt, *Chem. Eur. J.*, 2019, **25**, 6342–6348.

97 GaussView, Version 6, Dennington, Roy; Keith, Todd A.; Millam, John M. Semichem Inc., Shawnee Mission, KS, *Gaussian*, 2016.

98 L. Falivene, R. Credendino, A. Poater, A. Petta, L. Serra, R. Oliva, V. Scarano and L. Cavallo, *Organometallics*, 2016, **35**, 2286–2293.

99 L. Falivene, Z. Cao, A. Petta, L. Serra, A. Poater, R. Oliva, V. Scarano and L. Cavallo, *Nat. Chem.*, 2019, **11**, 872–879.

100 C. Ehm, A. Vittoria, G. P. Goryunov, V. V. Izmer, D. S. Kononovich, O. V. Samsonov, P. H. M. Budzelaar, A. Z. Voskoboynikov, V. Busico, D. V. Uborsky and R. Cipullo, *Dalton Trans.*, 2020, **49**, 10162–10172.

101 C. Ehm, A. Vittoria, G. P. Goryunov, V. V. Izmer, D. S. Kononovich, P. S. Kulyabin, R. Di Girolamo, P. H. M. Budzelaar, A. Z. Voskoboynikov, V. Busico, D. V. Uborsky and R. Cipullo, *Macromolecules*, 2020, **53**, 9325–9336.

102 C. Ehm, A. Vittoria, G. P. Goryunov, V. V. Izmer, D. S. Kononovich, O. V. Samsonov, R. Di Girolamo, P. H. M. Budzelaar, A. Z. Voskoboynikov, V. Busico, D. V. Uborsky and R. Cipullo, *Polymers*, 2020, **12**, 1005.

103 S. Grimme, R. Huenerbein and S. Ehrlich, *ChemPhysChem*, 2011, **12**, 1258–1261.

104 M. Trivedi, G. Singh, A. Kumar and N. P. Rath, *Dalton Trans.*, 2013, **42**, 12849–12852.

105 B. Zhu, X. Huang and X. Hao, *Dalton Trans.*, 2014, **43**, 16726–16736.

106 K. Mashima, K. Higashida, A. Iimuro, H. Nagae and Y. Kita, *Chem. Rec.*, 2016, **16**, 2585–2594.

107 S. A. Knott, J. N. Templeton, J. L. Durham, A. M. Howard, R. McDonald and L. F. Szczepura, *Dalton Trans.*, 2013, **42**, 8132–8139.

108 M. Herberhold, A. Goller and W. Milius, *Z. Anorg. Allg. Chem.*, 2003, **629**, 1162–1168.

109 K. Von Dahlen and J. Lorberth, *J. Organomet. Chem.*, 1974, **65**, 267–273.